AIAA JOURNAL
Vol. 31, No. 3, March 1993

Time-Resolved Infrared Emission Spectroscopy in High-Enthalpy Supersonic Air Flows

W. T. Rawlins,* T. E. Parker,† R. R. Foutter,‡ and M. G. Allen†
Physical Sciences, Inc., Andover, Massachusetts 01810

We describe a spectrally resolved infrared emission method for observing path-integrated number densities and temperatures in high-temperature supersonic flow on a time-continuous basis. We have conducted infrared emission measurements of the fundamental vibrational band of nitric oxide (NO) to determine NO number densities and vibrational temperatures in a high-temperature, Mach 3 air flow in the Physical Sciences, Inc. (PSI) shock-tunnel facility. A specially constructed infrared array spectrometer was used to observe spectral distributions of NO vibrational radiation between 5 and 7 μm. The instrument was calibrated on a conventional shock tube and was implemented on the PSI shock tunnel to diagnose the flow at the exit of a Mach 3 nozzle, as driven by a plenum of shock-heated air at 3000–4000 K and 10–40 atm. Simultaneous flowfield imaging of NO by planar laser-induced fluorescence verified flowfield uniformity and determined NO number densities in good agreement with the infrared results. The observed vibrational temperatures can be related to the flow temperatures through consideration of vibrational nonequilibrium effects, and the observed NO number densities can be related to total pressures and atomic oxygen number densities in the expanded flow. Comparisons of observed and predicted flow compositions are discussed.

Introduction

THE applications of nonintrusive, optical/spectroscopic molecular diagnostics have become an important part of supersonic combustion research, especially in support of hypersonic flow testing for the development of supersonic combusting ramjet (SCRAMJET) engines. As discussed in two companion papers,[1,2] pulsed laser-induced fluorescence methods can provide single-shot, instantaneous spatial distributions of individual species and temperatures in complex reacting flowfields. In addition, spectrally resolved line-of-sight techniques, such as passive emission or resonance absorption spectroscopy, can provide spatially integrated but continuously sampled information on flow composition and temperature. Such measurements are an important complement to instantaneous imaging, in that they provide a continuous and quantitative measure of the flowfield behavior with time throughout the test period. This paper describes observations of temperature and number density by infrared emission measurements of the fundamental vibrational band of nitric oxide (NO) in a high-temperature, Mach 3 air flow in the PSI shock-tunnel facility.

Simultaneous observations of the band shape and absolute radiance from vibrationally excited NO provide the column density (integral of the number density along the line of sight) and path-averaged vibrational temperature of NO in the flowfield. In our experiments, NO is formed at equilibrium levels in the high-temperature air in the plenum (3000–4500 K), and is not significantly depleted by chemical reactions in the supersonic expansion. Thus this species provides a convenient tracer for the number density and temperature of the air flow. Since the vibrational relaxation of NO is fast, the vibrational temperatures determined from infrared measurements closely approximate the kinetic temperatures in the gas flow. Furthermore, continuous monitoring of the NO emission characteristics provides a direct measure of flow onset, stability, and duration over the test period. The infrared measurements described in this paper were performed at the exit of a Mach 3 nozzle, in a region of spatially uniform flow as verified by ultraviolet planar laser-induced fluorescence (PLIF) imaging of NO.

Infrared emission from the fundamental ($\Delta v = 1$) vibrational band of NO originates near 5.3 μm (the center of the $v' \rightarrow v'' = 1 \rightarrow 0$ band), and extends to longer wavelengths as higher temperatures populate higher vibrational levels. This is illustrated in Fig. 1, which compares computed spectra of NO (v) emission at two different vibrational temperatures. The spectra in Fig. 1 were computed for an assumed spectral resolution of 0.1 μm, using the methods and spectroscopic constants described by Rawlins et al.[3] These spectra incorporate the contributions from higher vibrational levels, whose $\Delta v = 1$ emissions are shifted to progressively longer wavelengths, as illustrated by the bar graph in Fig. 2. These shifts come about because the molecule is an anharmonic oscillator, with the result that the energy spacing between adjacent vibrational levels becomes progressively smaller as the vibrational energy increases. Thus the shape of the long wavelength side of the band is highly sensitive to the high-level vibrational state populations and therefore to temperature, and measurements of the relative spectral intensities in this region will determine the vibrational temperature of the NO molecules in the field of view.

In addition, the absolute spectral intensities determine the column density or path-integrated number density of NO

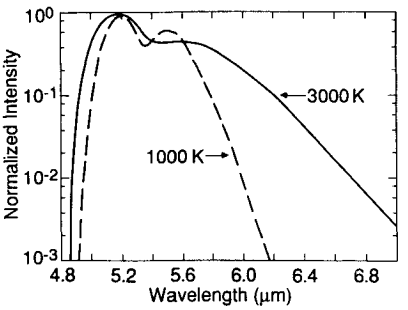

Fig. 1 Computed NO(v) emission spectra for two different vibrational temperatures (spectral resolution = 0.1 μm).

Presented as Paper 92-0140 at the AIAA 30th Aerospace Sciences Meeting, Reno, NV, Jan. 6–9, 1992; received Feb. 13, 1992; revision received July 9, 1992; accepted for publication July 10, 1992.

*Manager Chemical Sciences, 20 New England Business Center.
†Principal Research Scientist, 20 New England Business Center.
‡Senior Scientist, 20 New England Business Center.

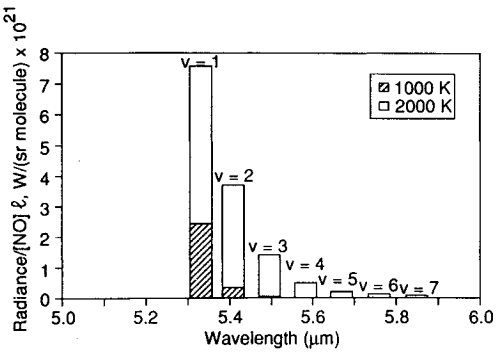

Fig. 2 Comparison of spectral contributions from NO(v) vibrational levels for two different vibrational temperatures.

molecules along the line of sight. For optically thin conditions, i.e., conditions where the observed radiation is not appreciably absorbed by the radiating species or by other species along the line of sight, the observed spectral intensity at a given wavelength is directly proportional to the column density of NO. For small NO column densities, the radiation on the long wavelength side of the band may become difficult to detect with adequate signal/noise ratio, and the measurements must be made nearer to the band center. For large NO column densities, the 1→0 contribution may become optically thick (i.e., self-absorbing through the 0→1 transition), and measurements must avoid this portion of the band. However, under such conditions the longer wavelength, higher v portion of the band will be readily detectable and still optically thin. The analysis can then be restricted to the optically thin portion of the band, providing useful results even when the 1→0 portion is optically thick. Thus the best measurement reliability and dynamic range can be attained through simultaneous monitoring of the entire spectral distribution of the band. In the present work, we have accomplished this by an infrared array spectrometer at low to moderate spectral resolution.

In the following sections, we discuss the experimental methods and conditions, the calibrations of the spectrometer, and the results of the measurements. We also discuss comparisons of NO number densities and temperatures measured by this method with those determined from PLIF images and predicted from kinetic flow model computations.

Experimental Methods

The hypersonic flow measurements reported here were conducted in a high-enthalpy shock tunnel described in detail in a companion paper.[1] The Mach 3 tunnel flow is driven by a plenum of shock-heated air (typically, 10–35 atm, 3000–4000 K) in the reflected shock region of a 15.6-cm i.d. shock tube. The gas, which contains N_2, O_2, NO, O, N, and N_2O at mole fractions near equilibrium values for the plenum conditions, expands through a two-dimensional half-nozzle to a uniform Mach 3 flow, typically at 0.3–1.0 atm and 1400–1700 K. The uniform flow further expands over a rearward facing step into a rectangular test section, where fuel is injected for combustion investigations. Optical stations at each of five axial locations along the tunnel provide optical access in two orthogonal directions so that line-of-sight and PLIF imaging measurements can be made at each location. The NO number density measurements reported here were performed in the uniform flow region, immediately after the full expansion point of the nozzle and upstream of the step, with no fuel injection.

Spectrally resolved NO vibrational emission was observed using a specially constructed infrared array spectrometer. This device consists of a liquid nitrogen cooled 12-element HgCdTe linear detector array (Infrared Associates) interfaced to a 0.35-m f/6.2 monochromator (McPherson 270), with a 30-groove/mm grating blazed at 5.5 μm. The resulting spectral resolution is nominally 0.19 μm/pixel. Each pixel in the array has a dedicated amplifier and digitizer providing synchronous collection of spectra at data rates of 125 kHz. The data were acquired and processed through a multichannel LeCroy/CAMAC data acquisition system interfaced to an IBM PC/AT computer. Absolute responsivity calibrations were performed with a temperature-controlled blackbody source. For the present measurements, the instrument was configured to obtain time-resolved, first-order spectra over the wavelength range 4.5–7.0 μm, encompassing the entire NO fundamental band. The field of view of the instrument was controlled using a folding imaging system consisting of a gold spherical mirror, focal length 10 cm, and a gold planar mirror. This optical system defined a collection volume in the tunnel of 3.1 × 3.1 mm at the tunnel centerline and 6.6 × 6.6 mm at the near and far edges, providing uniform sampling across the tunnel.

Prior to implementation of the spectrometer on the shock tunnel, the observed radiances and bandshapes were calibrated for NO number density and vibrational temperature by recording emission spectra for known amounts of NO (highly diluted in argon) shock-heated to known, constant temperatures in the reflected shock region of a conventional, 10.4-cm i.d. shock tube. These measurements were made at selected reflected shock temperatures of 800–2500 K, total pressures near 1 atm, and NO number densities near 10^{17} molecules/cm^3. The test section was scrupulously evacuated and baked to remove impurities, and "blank" shocks of argon test gas confirmed that there was no impurity radiation in the bandpass of interest. Nitric oxide was purified by passage through an Ascarite® column to remove higher oxides; gas purity was verified by infrared absorption spectroscopy. The optical measurements were made at an eight-port optical station located 3.5 cm upstream of the end wall. Additional measurements near 5 μm using a liquid nitrogen cooled, bandpass filtered InSb radiometer provided a crosscheck and verification of the spectrometer radiance measurements to better than ± 10%. As with the shock tunnel, the reflected shock conditions were computed from pressure transducer measurements of the incident shock velocities, giving shock temperatures accurate to ± 20 K.

Results and Analysis

Representative spectra of shock-heated NO/Ar mixtures are shown in Fig. 3. In each case, the radiances at each wavelength rise promptly upon arrival of the reflected shock, quickly reach a steady level, and remain constant for the duration of the reflected shock test time (approximately 2 ms). The observed spectra are obtained from the time-resolved data by averaging the observed radiances in each channel over the period of constant intensity. The observed radiances and spectral distributions between 4.9 and 6.6 μm are clearly due to NO, and are in excellent agreement with values computed using Boltzmann equilibrium vibrational populations together with the known spectroscopic constants and transition probabilities of NO (as documented in Ref. 3). The weak emission between 4.5 and 4.8 μm observed at higher temperatures can be ascribed to trace levels of N_2O which survived the NO purification procedure. More detailed spectral analysis of the data in Fig. 3, together with comparisons to predicted spectral distributions and structure, are presented in a separate publication.[4]

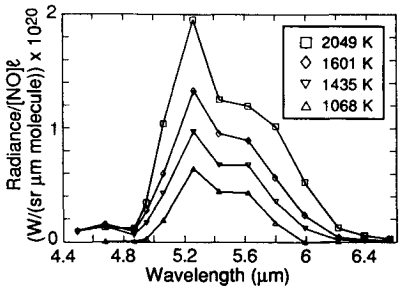

Fig. 3 Infrared spectra from shock-heated NO/Ar mixtures.

The observed integrated band intensities can be compared to predicted values in a straightforward manner. For optically thin conditions, the radiance integrated over the entire band, i.e., 4.9–6.6 μm, is given by

$$\frac{\int I_\lambda \, d\lambda}{[NO]\,\ell} = \frac{hc\nu}{4\pi} \sum_{v'=1}^{\infty} \left(e^{-E_{v'}/kT} / \sum_{v=0}^{\infty} e^{-E_v/kT}\right) A_{v'} \qquad (1)$$

where I_λ is the spectral radiance in $W/(cm^2 sr \mu m)$ at the wavelength λ, [NO] is the number density of NO in molecules/cm^3, ℓ is the path length (tube diameter) in cm, ν is the band-center transition frequency, E_v is the energy of vibrational level v, A_v is the band-averaged transition strength for emission from level v in s^{-1}, and the physical constants h, c, and k have their usual significance.

We have evaluated the right-hand side of Eq. (1) using the spectroscopic constants and transition strengths given in Ref. 3. It is particularly noteworthy that the transition strengths given in Ref. 3 are based on room temperature absorption data from Refs. 5 and 6. The predicted and observed intensities are compared in Fig. 4. The agreement is excellent over the entire temperature range of the present measurements, and signifies an accurate determination of the high-temperature band strength of NO which is consistent with room temperature data. A more complete analysis and discussion of this aspect of the results is presented elsewhere.[4]

The observed temperature dependence of optically thin radiance at several wavelengths is illustrated in Fig. 5. As expected from the fundamental relationships [cf. Eq. (1) and Ref. 7], the observed radiance at a given wavelength fits well to an expression of the form

$$\frac{I_\lambda}{[NO]\,\ell} = \alpha_\lambda \exp(-\beta_\lambda / T) \qquad (2)$$

with the characteristic exponential slope β increasing with increasing wavelength (higher vibrational level). Ratios of radiances at any two wavelengths are sensitive to temperature only, and are independent of [NO]

$$T = \frac{\beta_2 - \beta_1}{\ell n\,(I_1\alpha_2 / I_2\alpha_1)} \qquad (3)$$

Thus observations of the radiance ratios, under optically thin conditions, provide a determination of temperature using values of α_λ and β_λ determined empirically in the shock-tube calibrations. The temperature can then be applied to observations of spectral radiance at a given wavelength, via Eq. (2), to determine [NO].

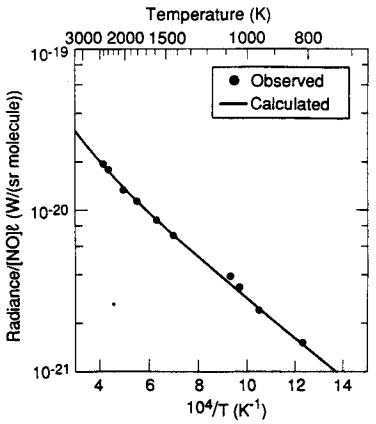

Fig. 4 Observed band integrated radiance compared to calculated values for NO.

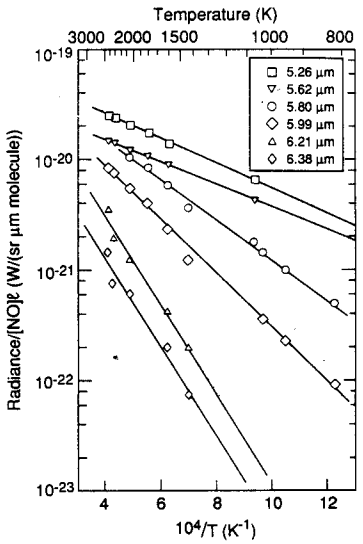

Fig. 5 Dependence of NO(v) radiances on temperature: lines represent least squares fits which determine the coefficients α_λ and β_λ.

The calibration data obtained in the shock tube correspond to equal vibrational and rotational temperatures. In nonequilibrium cases, where the vibrational and rotational "temperatures" are widely different, calibrations using equilibrium conditions are not applicable. In such a case, e.g., a vibrational distribution of ~2000 K and a rotational distribution of a few hundred K, the spectrum can be analyzed for both the vibrational and rotational distributions using a more complex spectral simulation/least-squares-fitting method developed and extensively employed by Rawlins and co-workers (e.g., Ref. 3 and citations therein). However, for the shock-tunnel conditions addressed here, the vibrational and rotational temperatures are different by only 15% or less (see Discussion), and the accuracy of the radiometric temperature determination is not affected by the use of equilibrium calibration data.

For some of the shock-tube calibration measurements, spectra were observed at sufficiently large NO number densities that the 1→0 transition was optically thick ($\approx 1 \times 10^{19}$ molecules/cm^2). This results in a nonlinear relationship between NO number density and the radiances at wavelengths between 5.0 and 5.8 μm, where the total intensity contains contributions from this band. That is, the intensity in this spectral region increases more slowly with increasing [NO], and the data points fall significantly below the lines in Fig. 5. However, wavelengths of 5.8 μm and above are not affected by the optically thick 1→0 band, and the corresponding radiances remain optically thin. Radiances at these wavelengths then continue to provide an accurate measure of NO number density and temperature, even when the main portion of the band is optically thick. While this strategy can also be applied to shock-tunnel measurements under optically thick conditions, the NO number densities and path lengths in our tunnel are small enough that the NO radiance is optically thin over the entire band.

An example series of NO spectra observed in the shock tunnel at the exit plane of the nozzle is shown in Fig. 6. In this

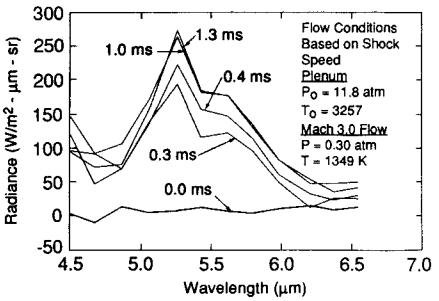

Fig. 6 NO spectra in the shock tunnel for several times during the flow: low pressure.

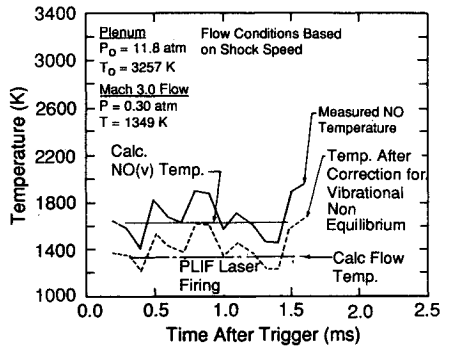

Fig. 7 Temperature determinations from the data of Fig. 6: low pressure.

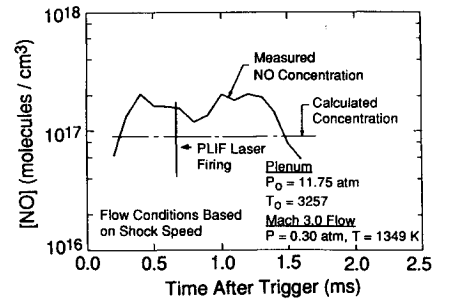

Fig. 8 NO concentration determined from Fig. 6: low pressure.

case, time-resolved 125-kHz data from the infrared spectrometer was digitally filtered with a 12.5-kHz sharp-cutoff, low-pass filter, and data points at 0.1-ms intervals were output to a separate data processing program. This particular experiment exhibited a significant continuum background contribution due to particulate in the flow (a problem which has subsequently been eliminated); our data processing corrects for this background by subtracting an interpolated background using 6.38 and 4.68 μm as end points. As illustrated by these measurements, an additional advantage of continuous spectral coverage is this ability to identify and remove contributions from particulates and other interfering radiators. The previously described calibration constants and Eq. (3) were used to determine the NO vibrational temperature as a function of time during the flow. The temperature at each time was in turn employed in Eq. (2) to determine the number density of NO in the flow using the radiance observed at 5.26 μm. Figure 7 illustrates the indicated vibrational temperatures for the spectra of Fig. 6, based on averages of the temperatures determined by ratioing 5.26 μm to 5.80 and 5.99 μm, and 5.43 to 5.80, 5.99, and 6.21 μm. Typical standard deviations of these averages were in the range 5–10%. The observed NO number densities for this case are shown in Fig. 8.

Also shown in Figs. 7 and 8 are the expected temperatures and number densities as computed from the plenum conditions using the kinetic flow model described in the Discussion. As described in more detail in the Discussion, the observed vibrational temperatures can be related to the flow temperatures through kinetic modeling of the vibrational relaxation process using previously reported kinetic data. It can be seen that when the anticipated 15% correction for vibrational nonequilibrium under these flow conditions is applied to the observed temperatures, the radiometric and predicted flow temperatures are in good agreement. However, the radiometric signal clearly indicates that the temperature and number density in the Mach 3 flow are by no means constant. These fluctuations may be attributable to variations in the plenum, e.g., a nonideal shock reflection off the nonplanar end wall or secondary reflections of the shock off the contact surface.

Figures 9 and 10 illustrate results from a shock-tunnel measurement at higher pressure and temperature. In this case the pressure in the plenum is high enough that no correction for vibrational nonequilibrium is required. The high temperatures and low number densities at early time signify the flow onset, when vibrational and chemical equilibrium in the plenum have not yet been attained. At late times, the temperature rises and the number density decreases as the pressure in the plenum is depleted. Thus continuous monitoring of the radiance permits clear identification of the period of relatively stable flow. Comparisons between observed and predicted temperatures and number densities will be discussed further in the next section.

The measurements reported in this paper were performed in uniform flowfields, where the variations in NO number density and temperature along the optical path are small. For such a case, the diagnostic samples a linear average of the properties along the line of sight for each point in time. This would not be true for a highly structured flowfield, where [NO] and T would vary significantly along the line of sight. In such a case the observed vibrational distribution would comprise a multimodal distribution of temperatures from different regions of the flow. While path-integrated column densities could be estimated with reasonable accuracy from a temperature-insensitive portion of the spectrum (e.g., near 5.2 μm), interpretation of temperatures would be more difficult. Companion spatial imaging measurements or flowfield structure models would enable spatial inversions of the observed column radiances to determine temperature profiles along the line of sight.

Concurrent measurements of the NO spatial distributions, in the same uniform flow region sampled by the infrared measurements, were made by planar laser-induced fluorescence (PLIF) using the pulsed laser excitation techniques described in detail in Ref. 2. These measurements, made at the flow time indicated in Fig. 8, provide an instantaneous view of the spatial uniformity of NO in the flowfield, as well as estimates of NO number densities via both the observed fluorescence yields and the resonance absorption of the laser beam. The PLIF images verify that the flow at the nozzle exit is spatially uniform, as expected. The observed attenuation of the laser sheet gives an estimated number density [NO] $\approx 3.2 \times 10^{17}$ molecules/cm^3, the observed fluorescence yields are consistent with [NO] $\approx 2.0 \times 10^{17}$ cm^{-3}, and the infrared emission measurement yields a value at the time of

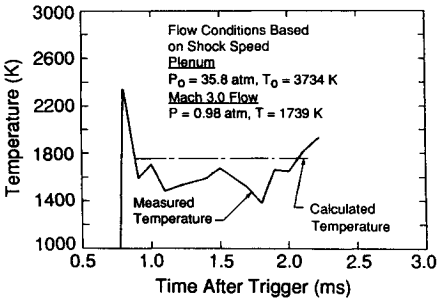

Fig. 9 Flow temperature from NO radiation in Mach 3.0 flow: high pressure.

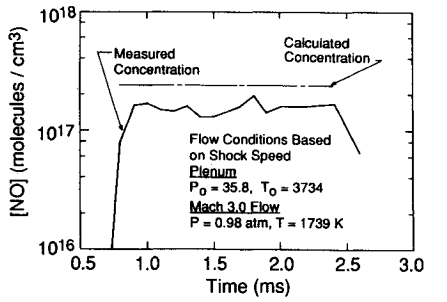

Fig. 10 NO concentration in the nozzle exit: high pressure.

the PLIF measurement of 1.5×10^{17}cm^{-3}. In view of the relatively large (factor of two to three) uncertainties in absorption coefficients, laser/absorber spectral overlap, laser energy delivered to the field of view, and quenching factors required to evaluate [NO] from the laser-based measurements, we consider these values to be in good agreement with the more quantitative value obtained by infrared emission. This comparison illustrates the utility of line-of-sight passive emission as a quantitative support diagnostic for instantaneous flowfield imaging measurements.

Discussion

It is instructive to compare the observed path-averaged NO(v) temperatures and number densities to values predicted for the expansion. In the absence of chemical reaction, the prediction of flow properties at the nozzle exit is a straightforward matter. However, finite rate chemistry and vibrational deactivation in the nozzle must be considered, and the resulting predictions have some uncertainty due to uncertainties in the chemical kinetics. For example, atom recombination in the nozzle tends to release energy into the flow, raising the temperature; and vibrational nonequilibrium causes a reduction in flow temperature due to storage of enthalpy in internal modes of the molecules. The degree to which these effects contribute depends upon the rate at which each process occurs as the gas flows through the nozzle. These rates will vary markedly with temperature, pressure, and gas composition, as illustrated in the following.

We have modeled the flow through the nozzle using a previously developed chemical kinetics code which simulates chemically reacting flow through a stream tube of specified geometry. The composition of the plenum gas was determined through separate kinetic modeling of the reflected shock region. In those calculations the initial reflected shock temperature was determined from pressure transducer measurements of the incident shock velocity, and the temperature and composition history of the shock-heated N_2/O_2 mixture was computed by the CHEMKIN chemical kinetics package.[8] In this case, dissociation of O_2 and N_2 and the subsequent formation of NO cause significant reductions in the initial temperature, and an equilibrium composition at the final temperature is quickly attained. For a 50-atm system, the period required for 85% of the temperature drop to occur is 1.2 ms at 2500 K, 0.18 ms at 3000 K, and less than 50μs at 3500 K. Thus the initial dissociation kinetics will result in transients at the onset of the flow in the tunnel, but the flow conditions will quickly relax to a steady level if the plenum temperature is high enough. We have used the predicted steady-state plenum conditions as starting points for the modeling of the nozzle flow.

The kinetic modeling employed the elementary reactions listed in Table 1, with temperature-dependent rate coefficients as recommended by Hanson and Salimian[9] and Baulch et al.[10,11] In addition, the vibrational relaxation of NO, N_2, and O_2 was treated using available data on the temperature-dependent collisional deactivation rate coefficients.[12-16] Although reactions of NO_2 and N_2O were included, the system can be adequately modeled by reactions (1), (2), (4), (6), and (7) alone. By far, the most important process affecting the nozzle flow predictions are the recombination of atomic oxygen and the collisional deactivation of NO(v) and $N_2(v)$.

Predicted flow profiles for the low- and high-pressure cases are shown in Figs. 11 and 12. The predicted exit plane temperatures and number densities are compared to the observations in Figs. 7-10 and in Table 2. At the lower pressure (11.8 atm in the plenum), only about 15% of the O recombines in the nozzle (primarily in the region immediately upstream of the throat), and the predicted exit conditions are primarily sensitive to vibrational nonequilibrium effects. In this case, the predicted and observed temperatures are in excellent agreement, while the predicted [NO] is about a factor of two below the observed mean number density. In the contrasting higher-pressure case (35.8 atm in the plenum), over 40% of the initial O is predicted to recombine to O_2, while the vibrational temperature is within 3% of the flow temperature. The predicted exit temperature and [NO] are significantly higher than the observed mean values.

Table 1 Elementary reactions used to model plenum and nozzle chemistry

Reaction	Reference for rate coefficient
1) $O_2 + M = O + O + M$	11
2) $N_2 + M = N + N + M$	10
3) $N_2O + M = N_2 + O + M$	9
4) $NO + M = N + O + M$	10
5) $NO_2 + M = NO + O + M$	10
6) $O + N_2 = NO + N$	9
7) $O + NO = N + O_2$	9
8) $N_2O + O = NO + NO$	9
9) $N_2O + O = N_2 + O_2$	9
10) $N + NO_2 = NO + NO$	10
11) $N + NO_2 = N_2O + O$	10
12) $O + NO_2 = NO + O_2$	10
13) $NO + NO + O_2 = NO_2 + NO_2$	10
14) $N + N_2O = N_2 + NO$	9
15) $NO + N_2O = N_2 + NO_2$	9
Vibrational deactivation	
NO(v) + N_2, O_2	16
NO(v) + NO	12
$O_2(v)$ + N_2, O_2	13
$O_2(v)$ + O	14
$N_2(v)$ + N_2, O_2	13
$N_2(v)$ + O	15

Table 2 Predicted and observed quantities at nozzle exit

	Computed		
	Finite rate chemistry	No chemistry	Observed
Plenum:11.8 atm 3257 K			
P, atm	0.30	0.31	
Mole fraction O	0.026	0.030	
Mole fraction NO	0.052	0.057	
T_{flow}, K	1349	1401	
T_{NO}, K	1611	1401	1700 ± 200
[NO], cm^{-3}	8.3×10^{16}	9.2×10^{16}	$(1.7 \pm 0.3) \times 10^{17}$
Plenum: 35.8 atm, 3734 K			
P, atm	0.98	0.95	
Mole fraction O	0.031	0.054	
Mole fraction NO	0.060	0.080	
T_{flow}, K	1739	1608	
T_{NO}, K	1789	1608	1600 ± 100
[NO], cm^{-3}	2.4×10^{17}	3.4×10^{17}	$(1.5 \pm 0.3) \times 10^{17}$

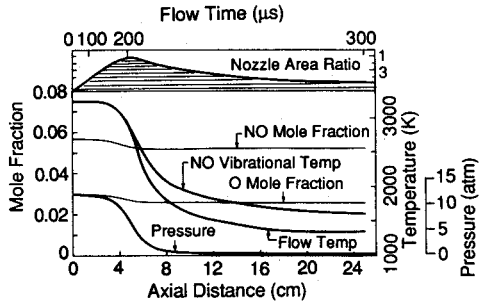

Fig. 11 Computed flow profiles, low pressure; fully relaxed plenum conditions: 3257 K, 11.8 atm.

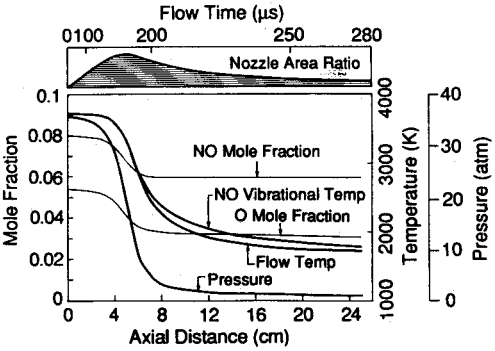

Fig. 12 Computed flow profiles, high pressure; fully relaxed plenum conditions: 3734 K, 35.8 atm.

The data illustrate that predicted and measured temperature and concentration values of the nozzle exit are not in strict agreement. We attribute this discrepancy to uncertainties in the high-temperature rate coefficients for both vibrational deactivation and chemical reaction processes and, in addition, note that the high-temperature plenum conditions may not be completely predictable with one-dimensional gas dynamics (due to the two dimensionality of the end wall). One of the key reactions is the recombination of atomic oxygen, which occurs in a small region upstream of the nozzle throat, at temperatures of 2500–3500 K. It appears from our temperature measurements that this rate must actually be slower than computed using the rate coefficients of Baulch et al.,[11] and that the actual O number densities exiting the nozzle may be considerably higher than we predict. [O] is a very important quantity to determine for studies of combustion in the downstream supersonic flow region, since atomic oxygen in the ambient flow is largely responsible for ignition of the fuel upon its injection into the flow. These considerations point to the need for more detailed experimental investigations in this temperature range, and emphasize the general necessity for in situ diagnostics of the flowfield composition to support model predictions.

Conclusions

We have described an infrared spectral emission method for monitoring flow composition and temperature in an air-driven, high-temperature supersonic flow on a continuous basis. We have implemented this method for observations of NO(v) radiation to determine NO number densities and vibrational temperatures in Mach 3 flows of partially dissociated air. Comparisons of the measured values to those predicted from model calculations indicate that the vibrational nonequilibrium effects can be quite accurately quantified to yield flow temperatures from the data, but that chemical reaction rate for modeling for these flow conditions has considerable uncertainty.

While the technique gives path-integrated information, it can be employed in a region of uniform flow or in concert with flowfield imaging measurements to determine local species number densities. The key to this approach is to obtain comprehensive spectral information using the multiplex advantage of an array spectrometer. This same general method can be applied to other infrared radiators present in the flow, and we are currently investigating its application of measurements of H_2O levels downstream of the fuel injection point.

Acknowledgment

This work was supported by the Air Force Wright Laboratory under Phase II SBIR Contract F33615-88-C-2907, John Smith, Contract Monitor.

References

[1]Parker, T. E., Allen, M. G., Reinecke, W. G., Legner, H. H., Foutter, R. R., and Rawlins, W. T., "High-Temperature Supersonic Combustion Testing with Optical Disgnosis," *Journal of Propulsion and Power* (to be published).

[2]Allen, M. G., Parker, T. E., Reinecke, W. G., Legner, H. H., Foutter, R. R., Rawlins, W. T., and Davis, S. J., "Fluorescence Imaging of OH and NO in a Model Supersonic Combustor," *AIAA Journal*, Vol. 31, No. 3, 1993, pp. 505–512.

[3]Rawlins, W. T., Fraser, M. E., and Miller, S. M., "Rovibrational Excitation of Nitric Oxide in the Reaction of O_2 with Metastable Atomic Nitrogen," *Journal of Physical Chemistry*, Vol. 93, No. 3, Feb. 1989, p. 1097.

[4]Rawlins, W. T., Foutter, R. R., and Parker, T. E., "Vibrational Band Strength and Temperatures of Nitric-Oxide by Time-Resolved Infrared Emission Spectroscopy in a Shock Tube," *Journal of Quantitative Spectroscopy and Radiative Transfer* (to be published).

[5]Mandin, J. Y., Amiot, C., and Guelachvili, G., "Intensity and Self Broadening Coefficient Measurements from Fourier Transform Spectra: Application to the Nitric Oxide Fundamental Band," *Annual Physics*, Vol. 5, June 1980, p. 91.

[6]Holland, R. F., Vasquez, M. C., Beattie, W. H., and McDowell, R. S., "Absorptivity of Nitric Oxide in the Fundamental Vibrational Band," *Journal of Quantitative Spectroscopy and Radiative Transfer*, Vol. 29, No. 5, May 1983, p. 435.

[7]Herzberg, G., "Wave Mechanics," *Molecular Spectra and Molecular Structure: I. Spectra of Diatomic Molecules*, 2nd ed., Van Nostrand, New York, 1950, pp. 18–21.

[8]Kee, R. J., Miller, J. A., and Jefferson, T. H., "CHEMKIN: A General Purpose, Problem Independent, Transportable, Fortran Chemical Kinetics Code Package," Sandia Lab., SAND 80-8003, Albuquerque, NM, March 1980.

[9]Hanson, R. K., and Salimian, S., "Survey of Rate Constants in the N/H/O System," *Combustion Chemistry*, edited by W. C. Gardiner Jr., Springer-Verlag, New York, 1984, pp. 361–421.

[10]Baulch, D. L., Drysdale, D. D., Horne, D. G., and Lloyd, A. C., *Evaluated Kinetic Data for High Temperature Reactions Vol. 2: Homogeneous Gas Phase Reactions of the H_2-N_2-O_2 System,* Butterworths, London, 1973.

[11]Baulch, D. L., Drysdale, D. D., Duxbury, J., and Grant, S., *Evaluated Kinetic Data for High Temperature Reactions. Vol. 3: Homogeneous Gas Phase Reactions of the O_2-O_3 System, the CO-O_2-H_2 System, and of Sulphur-Containing Species*, Butterworths, London, 1976.

[12]Wray, K. L., "Shock-Tube Study of the Vibrational Relaxation of Nitric Oxide," *Journal of Chemical Physics*, Vol. 36, No. 10, 1962, p. 2597.

[13]Millikan, R. C., and White, D. R., "Systematics of Vibrational Relaxation," *Journal of Chemical Physics*, Vol. 39, No. 12, 1963, p. 3209.

[14]Kiefer, J. H., and Lutz, R. W., "The Effect of Oxygen Atoms on the Vibrational Relaxation of Oxygen," *Eleventh Symposium (International) on Combustion*, Combustion Inst., Pittsburgh, PA, 1967, p. 67.

[15]Breshears, W. D., and Bird, P. F., "Effects of Oxygen Atoms on the Vibrational Relaxation of Nitrogen," *Journal of Chemical Physics*, Vol. 48, No. 10, 1968, p. 4768.

[16]Taylor, R. L., "Energy Transfer Processes in the Stratosphere," *Canadian Journal of Chemistry*, Vol. 52, No. 8 (Pt. 2), 1974, p. 1436.